Photoluminescence and the exciton-phonon coupling in hydrothermally grown ZnO

R. J. Mendelsberg*
Department of Physics and Astronomy, University of Canterbury, Christchurch, New Zealand and The MacDiarmid Institute for Advanced Materials and Nanotechnology, New Zealand

M. W. Allen and S. M. Durbin†
Department of Electrical and Computer Engineering, University of Canterbury, Christchurch, New Zealand and The MacDiarmid Institute for Advanced Materials and Nanotechnology, New Zealand

R. J. Reeves‡
Department of Physics and Astronomy, University of Canterbury, Christchurch, New Zealand and The MacDiarmid Institute for Advanced Materials and Nanotechnology, New Zealand

(Received 19 February 2010; published 17 May 2011)

Near band-edge photoluminescence (PL) from hydrothermally grown bulk ZnO was studied as a function of temperature along with the effects of simultaneous excitation with below-gap photons, allowing for accurate assignment of the emission features not possible from low-temperature data alone. Free exciton emission was clearly observed at low temperatures and dominated the PL spectrum above 100 K. Emission from *A* excitons bound to three neutral donors dominated the low-temperature PL spectrum. Recombination of *B* excitons bound to these same neutral donors were also identified along with *A* excitons bound to the donors in their ionized state. A clear difference in the redshift of free and bound excitons with increasing temperature was observed and attributed to reduced exciton-phonon coupling for the bound excitons. Additionally, Fano resonance of the 1-LO replica of the dominant bound *A* exciton was observed to reduce its PL intensity which can lead to the misidentification of the 2-LO replica as a donor-acceptor-pair transition.

DOI: 10.1103/PhysRevB.83.205202 PACS number(s): 78.55.Et, 71.35.−y, 78.55.Cr, 78.20.−e

I. INTRODUCTION

A wide, direct band gap, large exciton binding energy, and large spontaneous electrical polarization[1] make ZnO an ideal material for the next generation of optoelectronic and optomechanic devices. Nanoscale piezoelectric generators based on ZnO have already been demonstrated[2] as well as Cr-doped ZnO films showing simultaneous ferromagnetic and ferroelectric properties at room temperature.[3] However, despite being studied for several decades,[4] more information is needed concerning the nature of the optically and electrically active defects and impurities in ZnO to support efforts to realize potential ZnO based devices. The availability of high quality bulk ZnO single crystal substrates from several competing suppliers is a significant step forward. In particular, bulk wafers grown by the hydrothermal technique have recently attracted considerable attention, in part due to an inherent tendency to be heavily compensated by the presence of residual Na and Li acceptors.[5,6]

Photoluminescence (PL) spectroscopy is a probe of the electronic band structure in semiconductors and provides valuable information about the impurity content and crystal quality in a nondestructive way. In Si, which has an indirect gap, PL can detect impurity concentrations in the parts-per-billion range.[7] PL is even more useful for characterizing ZnO due to its direct band gap and large oscillator strength (two orders of magnitude higher than that of GaAs).[8] Over 15 excitonic features have been reported in the low-temperature PL spectrum of melt-grown[9] and vapor-transport-grown ZnO,[10] which reflects the variety of impurities that can be incorporated into bulk ZnO grown by different methods. Energetic splitting of the features is comparable to experimental uncertainties, which complicates identification and necessitates highly accurate spectrometers that are well calibrated. Diffusion studies[10] and radiotracer techniques[11] have been used to identify some of these features but many still have unknown chemical origins. Furthermore, the particular excitonic complexes responsible for the various sharp emissions are as yet unidentified or the subject of controversy. For neutral acceptor bound excitons the problem is of increased importance since their predicted energies lie in the same spectral region as excitons bound to commonly observed structural defects and deep donors. This means that care must be taken when using PL peaks to indicate that the elusive *p*-type doping has been achieved.

In this work, we report on the PL emission from the near band-edge (NBE) region of as-received bulk substrates grown by the hydrothermal technique (Tokyo Denpa Ltd., Japan). Room-temperature (0.51T) Hall-effect measurements indicate carrier concentrations of approximately 10^{13}–10^{14}cm^{-3}. The temperature and excitation intensity dependence of the emission was explored as well as the effects of simultaneous pumping with a below-gap laser. The richness of the NBE emissions and their close spacing challenge the determination of the absolute peak energy of any particular line. Furthermore, most studies on PL of ZnO are concerned with a relatively small number of samples. To address these issues, two different spectrometers were used to collect the PL signal from over 20 different samples cut from 14 different wafers. PL from several samples was also recorded more than once and as such, the whole data set gives an accurate picture of the uncertainty of the PL experiment and also accounts for the variation in the available ZnO crystals. Consequently, clear observation of subtle differences in the behavior of free and bound excitons in bulk ZnO is possible.

II. EXPERIMENT

Steady-state PL spectra were obtained from the as-received samples by excitation with a 20-mW He-Cd laser operating at 325 nm (3.815 eV). Unattenuated excitation intensity was 3 W/cm^2 and could be varied over several orders of magnitude using calibrated filters. For below-gap excitation, the 514.9-nm (2.407 eV) line of an Ar$^+$ laser was used. It was focused to an intensity of 60 W/cm^2 and was coincident with the He-Cd laser spot. The angle of incidence of both lasers was approximately 40°. All ZnO wafers in this study were *c*-plane oriented and the PL emission emitted along the *c* axis was collected from the Zn-polar face. Polarization of the laser was $\mathbf{E} \perp \mathbf{c}$ and the detection was done in the α geometry ($\mathbf{E} \perp \mathbf{c}$, $\mathbf{k} \parallel \mathbf{c}$, where **E** is the electric-field vector, **k** is the light wave vector, and **c** is directed along the *c* axis of the ZnO wurtzite structure).

Multiple samples were placed in a liquid-He-cooled cryostat with a built-in heater, allowing accurate temperature control from 3.5 to 300 K. PL emission was collected, collimated, and focused into either a Spex1700 monochromator with a 75-cm focal length and one 2400-line/mm UV blazed grating, or a Spex1403 double monochromator with a 2 × 85- cm focal length and two 1800-line/mm holographic diffraction gratings. The sampled bandwidth in the UV region was between 0.03 and 0.1 meV for the 1403 and 1700 spectrometers, respectively. In both cases, the signal was detected by the same photomultiplier tube operated in photon counting mode. The spectral response of each system is relatively flat over the narrow NBE region of ZnO so no intensity corrections were made to the spectra to avoid adding noise.

Wavelength calibration of the spectrometers was checked by scanning at least four known transitions of a low-pressure Hg and/or Ne lamp. Spectrometers were aligned with a known UV transition, and data from the Spex1700 required a wavelength dependent correction. Uncertainties on the absolute energy values were 0.5–1.0 meV due to fluctuations in ambient conditions from day to day. However, uncertainty on the difference in energy between two sharp excitonic features was between 0.2 and 0.5 meV depending on the sample, the specific features, and the spectrometer configuration. In most cases, uncertainty was limited by the samples since peak spacings as small as 0.05 meV can be reliably measured. the spectrometer choice for each experiment was based chiefly on the resolution–run-time tradeoff. The use of many samples and more than one instrument gave an in-depth understanding of the reproducibility of the experiment.

III. RESULTS AND ANALYSIS

For high quality crystals, free exciton emissions should always be identified first. Being an intrinsic property of the material, they are common to all samples and provide a reference for bound exciton identification. These emissions are usually the highest energy peaks which are still located below the band edge. Also, free exciton transitions are the last NBE peaks to disappear with increasing temperature since bound excitons become thermally delocalized from their binding centers. In ZnO, the 60-meV exciton binding energy results in free exciton luminescence, which has been observed up to 700 K.[12] Temperature-dependent PL is shown in Fig. 1(a) which shows typical intensity decay and redshift with increasing temperature.

Two of the high-energy features observed at 3.5 K (P_A and P^A) dominate the spectra at higher temperatures and they are accompanied by a third peak (PBN_A) which is obscured below 10 K. These three emissions are from free excitons, but due to the large oscillator strength in ZnO, the free excitons

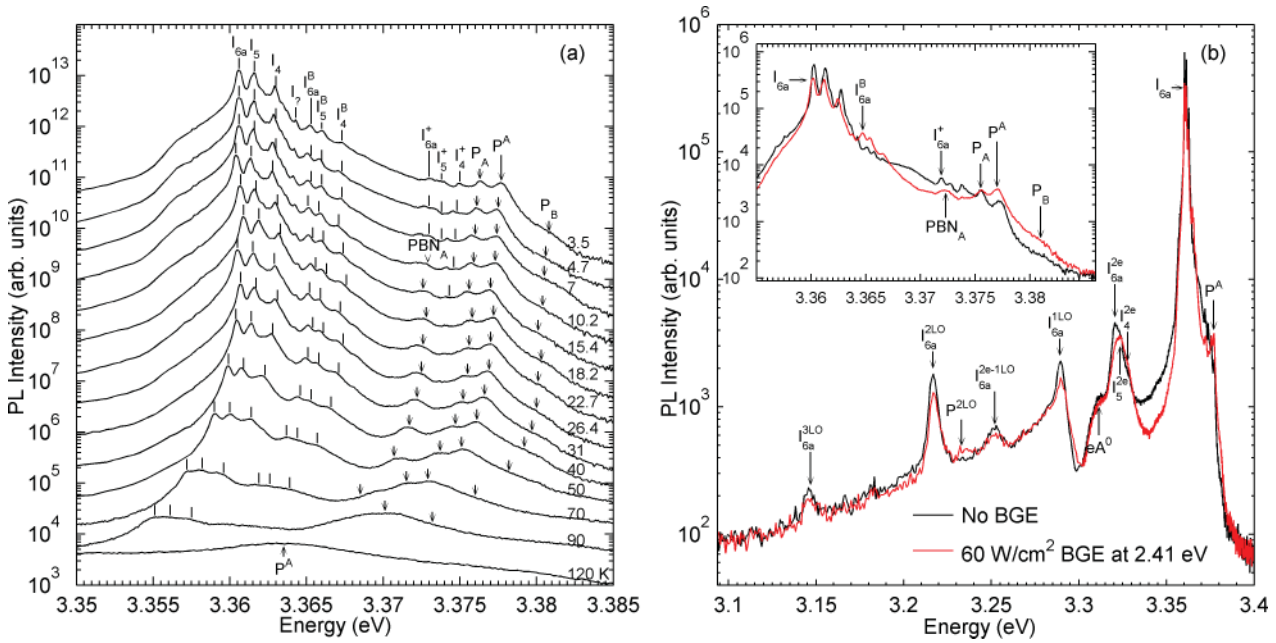

FIG. 1. (Color online) (a) Temperature-dependent PL from the Zn face (offset vertically for clarity). Lines with an arrowhead are a constant distance from P^A while the other markers are a constant distance from I_{6a}. (b) PL at 3.5 K with and without below-gap excitation (NBE region shown in inset).

TABLE I. Summary of the free exciton features in the low-temperature PL spectrum of bulk ZnO. The present work is the result of more than 30 measurements on 20 samples cut from 14 different hydrothermal wafers. The uncertainties represent the spread of the data.

Group	P_A (eV)	Notation	P^A (eV)	Notation	$P^A - P_A$ (meV)
Present work	3.3759 ± 0.0005	P_A	3.3776 ± 0.0005	P^A	1.7 ± 0.1
Reynolds *et al.*[14]	3.3775	Γ_5	3.3793	Γ_6	1.8
Meyer *et al.*[10]	3.3759	A_T	3.3772	A_L	1.3
Thomas[17a]	3.3758	A_m	3.3779	A_L	2.1
Teke *et al.*[9]	3.3757	$FX_A^{n=1}(\Gamma_5)$	3.3771	$FX_A^{n=1}(\Gamma_6)$	1.4
Klingshirn[13b]	3.3755	LPB	3.3774	UPB	1.9
Syrbu *et al.*[18]	3.3747	ω_t	3.3765	ω_L	1.8

[a]Measured from reflectance.
[b]Extracted from Fig. 15(a) of Ref. 13.

(with transverse character) couple with the photons to form polaritons.[13,14] This coupling splits the exciton dispersion curve into the upper and lower polariton branch (UPB and LPB, respectively) for the A, B, and C excitons. The peak marked P_A in Fig. 1 is the emission from the flat region of the lower A-polariton branch while P^A is the emission from the upper A-polariton branch.[13] PBN_A is a previously observed emission attributed to polaritons near the bottleneck region of the lower A-polariton branch.[14] The measured energy of these features, along with those reported in commonly cited publications, are shown in Table I. There is approximately 1-meV spread in the reported energies with good agreement for the splitting. However, not all reports agree on which free exciton or polariton complex is responsible for specific peaks. Some of the disagreement is likely due to the coincidental degeneracy of the so-called "longitudinal exciton,"[13,15] and some is residual confusion from the valence-band ordering controversy.[13,16]

The free exciton nature of these emissions is further confirmed by simultaneously pumping with below-gap excitation (BGE), as shown in Fig. 1(b). Free carriers are generated by the below-gap laser in a two-step process involving midgap defect states.[19] Photocurrent associated with this BGE free-carrier generation was separately observed in Schottky diodes fabricated on the same ZnO material.[20] No PL is observed under BGE only, indicating that photoexcited electrons and holes created by BGE do not form excitons. This means the free electron and the free hole lose correlation between photon absorptions and their high kinetic energy prevents subsequent exciton formation. These free carriers screen the Coulomb interaction, which reduces the trapping efficiency of binding centers for excitons. Thus bound exciton emission can be quenched by BGE and free exciton emission is unaffected or even enhanced since excitons which would normally bind to a center now have the opportunity to recombine freely. This can be observed in the inset of Fig. 1(b), which shows P^A and P_A gaining intensity while the three dominant bound exciton emissions are quenched. Also, BGE quenches three sharp peaks due to weakly bound excitons, allowing the PBN_A emission (unaffected or enhanced by the BGE) to be observed above the background. The high-energy shoulder near 3.383 eV also increases in intensity during BGE, suggesting the presence of emission from the lower B-polariton branch (P_B).

It should be noted that the peak labeled I_{6a}^B and the next two at higher energies are bound B-exciton peaks,[21] which surprisingly increase in intensity with BGE. The reason for increased bound B-exciton emission and quenched bound A-exciton emission is not yet understood but this phenomenon provides an easy way to separate the two. It should also be noted that the free carriers created by the BGE could be created by a single photon absorption at deep centers (precluding the creation of holes by the BGE). In both the one- and two-step processes, the steady-state carrier populations in deep centers are modified by the BGE, which may alter the radiative and nonradiative decay rates. In ZnO, it is known that nonradiative recombination dominates[22] and altering its impact may have different influences over the PL emission for free and bound excitons. This may be as important as carrier screening for time integrated PL observations of free and bound excitons.

After identifying the free exciton features, the other low-temperature UV emissions can be confidently identified as neutral and ionized donor bound excitons (D^0X and D^+X, respectively). Since peak spacings are more accurately measured than absolute peak positions, the localization energy E_{Loc} (measured as the energetic spacing between P_A and the bound exciton) represents the most reliable way to quickly identify previously reported bound exciton emissions. Peak positions and localization energies are shown in Table II and uncertainties indicate the spread of over 30 measurements. The best overall agreement for the localization energies measured in this work and those measured by Meyer *et al.*[10] was found by assigning the three dominant features to the I_4, I_5, and I_{6a} excitons. These excitons have been previously assigned as D^0X complexes of A excitons bound to neutral hydrogen, unknown, and aluminum donors, respectively.[10] Al impurities are introduced from the polycrystalline ZnO source material and hydrogen (along with Li and Na) from the mineralizers used in the hydrothermal growth process.[23] D^+X counterparts for the dominant D^0X recombinations were observed, labeled as I_x^+, which die out very quickly with temperature due to their small localization energies. The appearance of D^+X recombination indicates the presence of residual acceptors (likely Na and Li) which are compensating the donors. This compensation results in a population of ionized donors at cryogenic temperatures where thermal ionization is prevented. It should be noted that photoionization by the UV laser is

TABLE II. Summary of the bound exciton features (and PBN_A) in the low-temperature PL spectrum of bulk ZnO. The present work is the result of more than 30 measurements on 20 samples cut from 14 different hydrothermal wafers. The uncertainties represent the spread of the data, which includes between 9 and 20 data points for each exciton complex. Energy is in eV and E_{Loc} is in meV.

	Present work		Meyer *et al.*[10]		Teke *et al.*[9]		
Line	Energy[a]	E_{Loc}	Energy	E_{Loc}	Energy	E_{Loc}	Notation
P_A	3.3759		3.3759 (A_T)		3.3757		$FX_A^{n=1}(\Gamma_5)$
PBN_A	3.3727	3.2 ± 0.3[b]			3.3724	3.3	$D_2^0X_B$
I_4^+	3.3743	1.6 ± 0.1					
I_{4a}^+					3.3740	1.7	LPB_A
I_5^+	3.3731	2.8 ± 0.2					
I_{6a}^+ (I_0)	3.3723	3.6 ± 0.1	3.3725	3.4			
I_4^B	3.3667	9.2 ± 0.2[b]					
I_{4a}^B					3.3664	9.3	$D_5^0X_A$
I_5^B	3.3656	10.3 ± 0.1[b]					
I_{6a}^B	3.3649	11.0 ± 0.1[b]	3.3651	10.8	3.3650	10.7	$D_4^0X_A$
$I_?$	3.3637	12.2 ± 0.3					
I_4	3.3625	13.4 ± 0.2	3.3628	13.1			
I_{4a}					3.3618	13.9	$D_3^0X_A$
I_5	3.3612	14.7 ± 0.1	3.3614	14.5			
I_{6a}	3.3604	15.5 ± 0.1	3.3604	15.5	3.3605	15.2	$D_2^0X_A$
I_8			3.3598	16.1	3.3598	15.9	$D_1^0X_A$

[a]Based on the average spacing with P_A as listed in the third column as E_{Loc}.
[b]Here E_{Loc} is not a localization energy and is just the spacing with P_A since PBN_A is not a bound exciton.

minimal as indicated by the linear dependence of the D^+X complexes on UV excitation intensity (not shown here).

B-exciton counterparts to the dominant D^0X recombinations were also observed, spaced roughly 4.5 meV above the corresponding bound A excitons and labeled I_x^B. The 4.5-meV spacing agrees well with the splitting of the A- and B-valence bands reported by Meyer *et al.*[10] but differs considerably from the 12 meV reported by Teke *et al.*[9] This inconsistency in the reported splittings may be due to the large longitudinal-transverse splitting of the B excitons.[18] Confidence in the I_x^B assignments is obtained by noting that they show essentially the same decay in intensity with temperature as the I_x peaks.

The intensity of free and bound excitonic PL recombinations as a function of temperature can be described by an Arrhenius-type decay given by[24]

$$I(T) = \frac{I(0)}{1 + A\exp\left(\frac{-E_a}{k_B T}\right)}, \quad (1)$$

where $I(0)$ is the intensity at $T = 0$ K, A is a constant relating to the efficiency of the decay channel, k_B is the Boltzmann constant, and E_a is the activation energy of the decay channel. An Arrhenius plot of the absolute peak intensities is shown in Fig. 2 with the solid lines indicating the weighted-least-squares fit of Eq. (1). The best-fit activation energy of I_{6a} was 12.7 ± 0.1 meV and a value of 12 ± 2 meV was obtained for I_{6a}^B. Similar values are found for the I_4, I_5, I_4^B, and I_5^B peaks, confirming the I_x^B assignments.

Further confirmation of the I_x^B assignments is provided by noting that bound A excitons at the same energy as the I_x^B excitons would decay noticeably faster with temperature than was observed due to low localization energies. The peak marked as $I_?$ in Fig. 1(a) is a bound A exciton which does exactly that. By 40 K $I_?$ is unresolvable, dying out noticeably quicker than the I_x and I_x^B emissions on either side. Pb, a common impurity in many materials, is a possible origin of $I_?$ since the same excitonic peak with a localization energy of 12.2 ± 0.3 meV was induced by Pb implantation into hydrothermal ZnO.[25] Recent measurements (to be published) show that $I_?$ is not present in Bi-implanted ZnO, ruling out a structural defect as the origin of $I_?$.

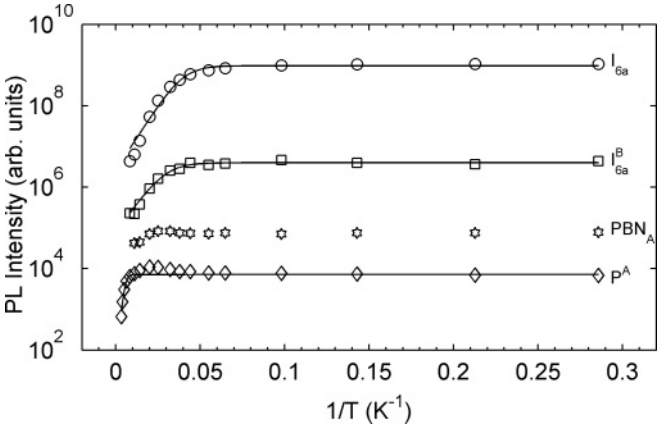

FIG. 2. Arrhenius plot of the absolute PL intensities. Straight lines are the $\sqrt{I(T)}$-weighted least-squares fit of Eq. (1).

It should be noted that Meyer *et al.*[10] observed an initial increase in PL intensity from the I_x^{B} peaks with increasing temperature in their study (vapor phase grown ZnO) and attributed it to thermal excitation of the A excitons to the B-valence band. Such an increase was only observed in one hydrothermally grown sample (from a recently grown batch) studied thus far, but it was observed for the B excitons in melt-grown wafers from Cermet (not shown here). Also, in the melt-grown ZnO the B-exciton peaks show an increase when subjected to BGE.

For all the fits, $\sqrt{I(T)}$ was used as the weighting, which assumes that repeated measurements of the PL intensity at a single energy will follow a Poisson distribution.[26] Accordingly, an activation energy of 80 ± 10 meV was extracted from the fit to the six high-temperature data points of P^A, in reasonable agreement with its binding energy of 60 meV. Despite using only the high-temperature data for the fit, the overestimation may be due to the increase in intensity of P^A as temperature is initially raised due to the thermal delocalization of the bound excitons. This initial intensity increase also occurs for PBN_A, which is shown in Fig. 2, further confirming its free exciton nature.

Violet emission from the Tokyo Denpa material is shown in Fig. 1(b) and consists of the two-electron-satellite (TES) transitions from the D^0X complexes, labeled I_x^{2e}, and the LO-phonon replicas from I_{6a} spaced 72 meV apart and labeled $I_{6a}^{m\mathrm{LO}}$. With BGE, the second LO replica of the free exciton-polariton peaks (P^{2LO}) gained intensity while the I_{6a}^{mLO} peaks lost intensity, as expected. A free electron to neutral acceptor transition, eA^0, was observed around 3.31 eV, which has been previously attributed to acceptor like basal-plane stacking faults.[27] Such nonexcitonic, defect related peaks are unaffected by the BGE as long as the trapping centers are not created or destroyed by the below-gap photons. Another such defect peak is likely underlying the TES emission, considering the small effect BGE has on the TES band.

The sharp dip in the spectra around 3.3 eV can be explained by quantum-mechanical Fano resonance,[28] which has been previously identified in high quality ZnO.[29] Fano resonance significantly reduces the intensity of I_{6a}^{1LO} and has led some authors to incorrectly assign I_{6a}^{2LO} as a donor-acceptor-pair (DAP) recombination.[9,10] Correct identification of DAP peaks in this region is crucial for accurate analysis of luminescence from p-type samples.

IV. DISCUSSION

Table II shows the connections between the emission measured in this work, that measured by Meyer *et al.*[10] in vapor phase material, and the emissions observed by Teke *et al.*[9] in melt grown wafers from Cermet Inc.[30] The common feature between the three materials is the Al-related I_{6a} peak and its B-exciton counterpart, which is not surprising since Al is an abundant element which easily finds its way into ZnO. I_8, which is known to be Ga related,[10] was not observed in the Tokyo Denpa material but it was a dominant feature in the PL of the vapor phase and melt grown wafers. The H-related I_4 emission was not observed in the melt grown material, but a peak with a slightly lower energy (labeled $D_3^0X_A$ by Teke *et al.*[9]) was present which can be labeled I_{4a} in line with the traditional I notation (see Table II and Ref. 10). Melt grown ZnO contains the least hydrogen since no mineralizers or carrier gases are used during growth.[30]

Comparing the line shape of the PL in the present work to that reported by Teke *et al.*,[9] we note that their $D_4^0X_A$ line is 4.5 meV above $D_2^0X_A$. The same spacing also occurs between $D_5^0X_A$ and $D_3^0X_A$. Rather than introducing new donor species the alternative interpretation is that $D_4^0X_A$ and $D_5^0X_A$ are the recombinations associated with the B-valence band,[21] i.e., I_{6a}^B and I_{4a}^B. Furthermore, comparison of the spacings shown in Table II also indicates that the PBN_A peak was assigned as a D^0X complex by Teke *et al.*[9] and a D^+X complex was assigned as PBN_A.

Typical redshifting with increasing temperature was observed for all the excitonic features, with a small difference in the shift between the free and bound excitons. Free exciton energies follow the band gap with changing temperature. It is generally accepted that lattice dilation and the electron-phonon interaction cause the redshift in the band gap of semiconductors, with the latter being the dominant contribution.[31,32] In fact, good fits to experimental data can be obtained by neglecting lattice dilation completely.[33,34] A useful model which only accounts for the electron-phonon interaction was first proposed by Viña *et al.*[34] and is given by

$$E_{\mathrm{g}}(T) = E_{\mathrm{g}}(0) - \frac{\alpha\theta}{\exp(\theta/T) - 1}, \tag{2}$$

where $E_{\mathrm{g}}(0)$ is the emission energy at $T = 0\,K$, α is proportional to the electron-phonon coupling, and θ is the effective phonon temperature. Exciton-phonon coupling is proportional to the electron-phonon coupling and thus, for excitonic transitions, α represents the effective exciton-phonon coupling strength. Figure 3 shows the energy shift of P_A and I_5 as a function of temperature with the dotted lines showing the weighted least-squares fit of Eq. (2). Also shown are the data from a melt grown wafer (Cermet). The uncertainties shown in Fig. 3 were used for the weighting and represent machine errors at low temperature. They expand as temperature increases due to error(s) in locating the peak maximum as the peaks broaden

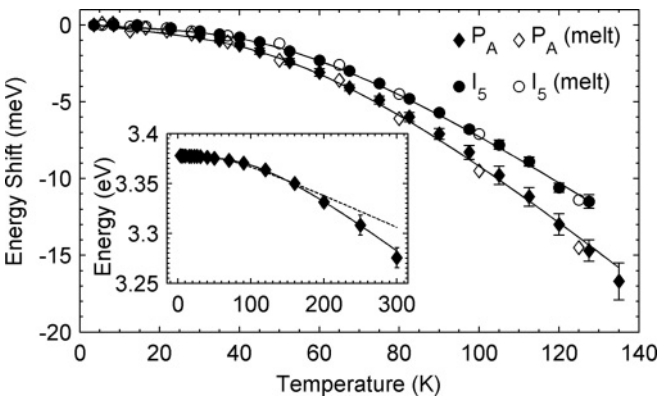

FIG. 3. Energy shift of the P_A (left axis) and I_5 (right axis) excitons. Data for a melt grown wafer are also shown. Full temperature range measurement of the energy shift of a different hydrothermal sample is shown in the inset with the lines showing the least-squares fit of Eqs. (2) (dotted) and (3) (solid).

TABLE III. Fitted parameters to the shift of the exciton emission energy with temperature.

Model	Parameter	P_A	I_5
Eq. (2)	$E(0)$ (eV)	3.3761 ± 0.0003	3.3622 ± 0.0003
	α (eV/K)	$(3 \pm 1) \times 10^{-4}$	$(1.3 \pm 0.3) \times 10^{-4}$
	θ (K)	200 ± 40	145 ± 15
	χ^2_R	2.8	0.5
Eq. (3)	$E(0)$ (eV)	3.3769 ± 0.0003	3.3620 ± 0.0006
	U (eV/K)	$(5 \pm 2) \times 10^{-5}$	$(1 \pm 5) \times 10^{-6}$
	α (eV/K)	$(5 \pm 2) \times 10^{-4}$	$(1.4 \pm 0.5) \times 10^{-4}$
	θ (K)	370 ± 80	100 ± 80
	χ^2_R	0.7	0.4

and converge. Fitted parameters along with the 95% confidence bounds are shown in Table III.

When ignoring the energy uncertainties, Eq. (2) gives an excellent fit (not shown) but as can be seen in the inset of Fig. 3, weighting the fit of Eq. (2) with the uncertainties results in a relatively poor looking fit. A much better weighted fit to the data can be obtained by accounting for the effect of lattice dilation as

$$E_g(T) = E_g(0) - UT - \frac{\alpha\theta}{\exp(\theta/T) - 1}, \tag{3}$$

where U is the lattice dilation constant. This model is essentially the same as that proposed by Manoogian *et al.*,[35] the only differences being that lattice dilation is assumed to be linearly dependent on temperature, and the exciton-phonon term is written in the equivalent, yet more intuitive Bose-Einstein form.[35] The solid lines in Fig. 3 are the weighted least-squares fit of Eq. (3) and the fitted parameters are shown in Table III. Also listed in the table are the reduced χ^2 parameters. χ^2_R can be used to quantitatively compare fits of similar models when the number of parameters is not constant,[26] such as the case for Eqs. (2) and (3). χ^2_R is also the parameter that is minimized during the weighted least-squares fitting.

A fourfold decrease in χ^2_R was observed for the fit to the P_A data when the U parameter was added. A much better match to the curvature in the data was also obtained over the entire temperature range. Roughly the same decrease in χ^2_R was observed when only the data up to 135 K was used for the fit, which was the same temperature range as the I_5 data. Hence the effect of lattice dilation on the band gap and free exciton energy in ZnO cannot be ignored and contributes 15 ± 3 meV of the redshift at 300 K (about 15%).

In contrast, the bound excitons all follow a different temperature dependence and have a significantly lower U value. A minimal reduction in the χ^2_R parameter was seen for the fit of I_5 when the U parameter was added and essentially identical α and θ values were also fit by both models to I_{6a}. At 125 K lattice dilation contributes 7 ± 3 meV to the redshift of the free exciton energy, comparable to the 4 ± 2 meV decrease in localization energy observed for I_5. This provides evidence that bound excitons are less sensitive to the effects of lattice dilation than free excitons.

Table III also shows a significantly reduced exciton-phonon coupling (α) for the bound excitons compared to the free excitons, consistent with our previous reports on ZnO nanostructures.[25] Reduced coupling to the phonons can be explained by the localized nature of the bound exciton wave function. Free excitons can be described by Wannier functions[36] which have an extended Bloch-like component. They interact with the lattice as a whole, resulting in large spatial overlaps with the phonon wave functions. Wave functions of donor bound excitons can be approximated by the product of a free exciton wave function centered near the impurity, the hydrogeniclike wave function of the donor electron in the $1s$ ground state, and an envelope function describing the exciton's orbit around the donor.[37] The extra factors significantly reduce the extended nature of the free exciton component, decreasing overlaps with the phonon wave functions, which reduces the exciton-phonon coupling for bound excitons. Such localization may also shield the bound excitons from the effects of lattice dilation since they encompass a much smaller number of lattice sites than the free excitons.

Another indicator of the strength of the exciton-phonon coupling is the Huang-Rhys factor S. Using the Frank-Condon approximation, the intensity ratio of the mth LO-phonon replica to the zero-phonon line (ZPL) of an emission peak is given by[38]

$$\frac{I_m}{I_0} = \frac{S^m}{m!}e^{-S} \quad \text{for } m = 1,2,3\ldots. \tag{4}$$

Here, S represents the average number of phonons produced during radiative recombination of a given transition and is directly proportional to the exciton-phonon coupling strength. This equation and one without the e^{-S} factor have been applied to other material systems including ZnSe[39] and AlN.[40] However, before extracting S factors, the LO replicas must be confidently identified. This can be problematic for ZnO since these features are in the same region of the spectrum as several DAP transitions.[38] PL from this region of the spectrum, taken from 3.5–70 K, is shown in Fig. 4. For the replicas from the polaritonic peaks (P^{xLO}), the arrows in the figure were placed according to the expected temperature shift of the LO replicas given by[9]

$$E_{m\mathrm{LO}}(T) = E_{\mathrm{ZPL}}(T) - m\hbar\omega_{\mathrm{LO}} + \left(L + \frac{1}{2}\right)k_B T, \tag{5}$$

where $E_{\mathrm{ZPL}}(T)$ is the energy of the ZPL at temperature T, $\hbar\omega_{\mathrm{LO}}$ is the LO-phonon energy of 72meV, and L is either 0 or 1 depending on if the mLO transition probability depends on the kinetic energy of the exciton. For the 1- and 2-LO replicas it is known that $L = 1$ and $L = 0$, respectively,[9] and good predictions are made by assuming $L = 0$ for $m = 3$. Furthermore, these features have the characteristic asymmetric line shape previously observed for LO replicas from free excitons in ZnO.[41] Strictly speaking, Eq. (5) applies only to free excitons but Fig. 4 shows that it also seems to predict the energy of the bound excitons and their TES transitions reasonably well.

At 4 K, a series of peaks spaced 72 meV from I_{6a} can be observed and are attributed to its LO-phonon replicas (I_{6a}^{xLO}). As mentioned previously, Fano resonance can explain the decreased intensity of the I_{6a}^{1LO} emission.[29] This is problematic

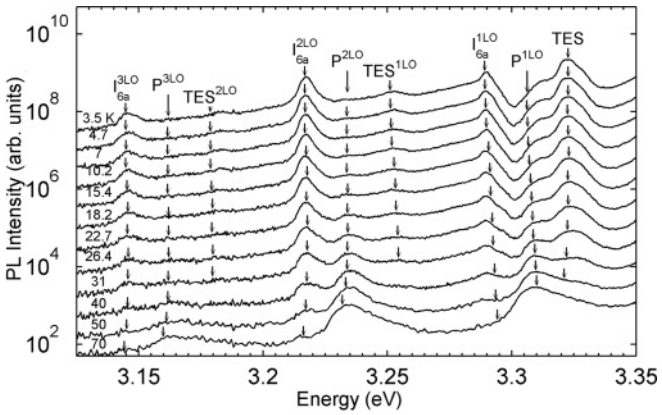

FIG. 4. Temperature-dependent PL from Tokyo Denpa ZnO in the violet region (offset vertically for clarity).

since it often leads to misidentification of the 2-LO replica as a DAP transition. Fano resonance is a quantum-mechanical phenomena that occurs when a discrete level exists on top of a continuum of states with which it can interact.[28] As pointed out by Jin and Xu,[29] it occurs in polar semiconductors like ZnO and GaN since the exciton-LO-phonon state sits on top of the continuum of exciton-acoustic-phonon states.

Further confidence in the LO-phonon identification comes from power dependent PL of I_{6a}^{2LO}, as shown in Fig. 5(a). DAP transitions are expected to blueshift with increasing excitation intensity,[38] which is clearly not the case for I_{6a}^{2LO}. Moreover, defect related emission intensity shows a sublinear dependence on the excitation intensity[42] and the intensity of I_{6a}^{2LO} shows linear dependence. Furthermore, an Arrhenius fit of the decay of intensity of I_{6a}^{2LO} with increasing temperature using Eq. (1) gives an activation energy of 7 ± 1 meV, less than that found for the zero-phonon line but significantly less than the 40–60 meV expected for DAP transitions.

With the LO replicas unambiguously identified, the Huang-Rhys factor S can be extracted from a least-squares fit to the measured intensity ratios as shown in Fig. 5(b). Most groups estimate S by the intensity ratio of the 1-LO replica only. The least-squares approach used here encompasses all observed replicas, allowing a more accurate estimate of the uncertainty in S. For P^A, the intensity ratio of the 0-, 1-, 2-, and 3-LO replicas at 70 K was used for the fit and resulted in $S = 0.66 \pm 0.09$. Ignoring the ZPL of the polaritonic peaks, to avoid any possible effects of reabsorption, gives a similar S value. Calculations at higher temperatures show values also falling in this range. For I_{6a}, only the intensity ratios of the 0-, 2-, and 3-LO replicas (at 3.5 K) were used in the fit resulting in $S = 0.12 \pm 0.04$. From the data in Fig. 5(b) it can be seen that Fano resonance quenches the I_{6a}^{1LO} intensity by a factor of 19. The same S factor is calculated if I_{6a}^{2LO} is incorrectly assumed to be the ZPL of a DAP recombination. DAP transitions are strongly coupled to the phonons with S factors typically around 0.4,[38] providing further quantitative evidence that I_{6a}^{2LO} is not a DAP transition. On another note, the extracted S factors indicate that P^A is coupled to the phonons 6 ± 2 times stronger than I_{6a}. This is in agreement with the α values extracted from Eqs. (2) and (3), which implies 4 ± 1 times the exciton-phonon coupling strength for P^A.

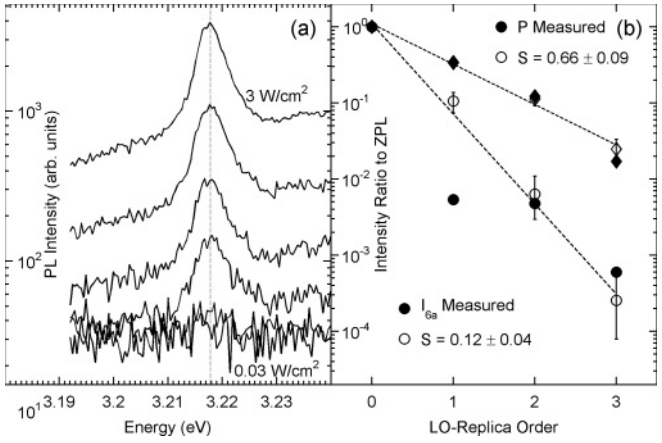

FIG. 5. (a) Power-dependent PL of I_{6a}^{2LO}, taken at 3.5 K, showing no blueshift and a linear dependence on excitation power. (b) Intensity ratios of the phonon replicas of P^A and I_{6a} to the zero-phonon line (ZPL) with calculated S values from the best fit of Eq. (4). Dotted lines show an exponential fit to the calculated data as a guide to the eye.

V. CONCLUSIONS

Temperature-dependent PL measurements were combined with a simultaneous BGE experiment and power dependent PL observations to understand the PL spectrum of bulk hydrothermal ZnO. At low temperature, emission from the upper and lower A-polariton branches was clearly observed. D^0X complexes dominated the low-temperature PL spectra and were attributed to A excitons bound to neutral hydrogen, unknown, and aluminum donors. Also observed were recombinations of B excitons bound to these same donors and A excitons bound to their ionized state. After establishing the connection between the D^0X, D^+X, and bound B excitons, another D^0X transition was identified with a localization energy of 12.2 ± 0.2 meV and was possibly due to Pb donors.

Careful analysis of the redshift of the PL features with increasing temperature showed a measurable difference between the free and bound excitons. It was shown that lattice dilation cannot be ignored for free exciton emission and contributes about 15% of the redshift at 300 K. However, lattice dilation may not affect the bound excitons as much. Exciton-phonon coupling was four to six times stronger for free excitons compared to the bound excitons. Despite the reduced coupling, Fano resonance was observed for the 1-LO replica of the I_{6a}^{1LO} emission, reducing its PL emission intensity by an experimentally determined factor of about 20 due to Fano resonance. This has previously led to misidentification of the I_{6a}^{2LO} as a donor-acceptor pair transition, which is particularly relevant for ZnO showing possible p-type behavior.

ACKNOWLEDGMENTS

The authors would like to acknowledge Paul Miller, Russel Gillard, Geoff Graham, and Bob Flygenring for their assistance. This work was supported in part by Marsden Fund Grant No. UOC0604 and the MacDiarmid Institute for Advanced Materials and Nanotechnology.

*Present Address: Lawrence Berkeley National Laboratory, Material Science Division, Berkeley, CA 94720.
†Present Address: Department of Electrical Engineering and Department of Physics, State University of New York at Buffalo, Buffalo, NY 14260.
‡roger.reeves@canterbury.ac.nz

[1]W. Glück, Solid State Commun. **8**, 1831 (1970).
[2]Z. Wang, Adv. Funct. Mater. **18**, 3553 (2008).
[3]Y. Yang, C. Zhong, X. Wang, B. He, S. Wei, F. Zeng, and F. Pan, J. Appl. Phys. **104**, 064102 (2008).
[4]E. Tomzig and R. Helbig, J. Lumin. **14**, 403 (1976).
[5]D. Zwingel and F. Gärtner, Solid State Commun. **14**, 45 (1974).
[6]D. Zwingel, J. Lumin. **5**, 385 (1972).
[7]M. Tajima and M. Nomura, Jpn. J. Appl. Phys. **20**, L697 (1981).
[8]M. Zamfirescu, A. Kavokin, B. Gil, G. Malpuech, and M. Kaliteevski, Phys. Rev. B **65**, 161205 (2002).
[9]A. Teke, U. Özgür, S. Doğan, X. Gu, H. Morkoç, B. Nemeth, J. Nause, and H. O. Everitt, Phys. Rev. B **70**, 195207 (2004).
[10]B. Meyer *et al*., Phys. Status Solidi B **241**, 231 (2004).
[11]K. Johnston, M. O. Henry, D. McCabe, E. McGlynn, M. Dietrich, E. Alves, and M. Xia, Phys. Rev. B **73**, 165212 (2006).
[12]X.-B. Chen, J. Huso, J. Morrison, and L. Bergman, J. Appl. Phys. **102**, 116105 (2007).
[13]C. Klingshirn, Phys. Status Solidi B **244**, 3027 (2007).
[14]D. Reynolds, D. Look, B. Jogai, and T. Collins, Appl. Phys. Lett. **79**, 3794 (2001).
[15]J. Hopfield and D. Thomas, J. Phys. Chem. Solids **12**, 276 (1960).
[16]W. R. L. Lambrecht, A. V. Rodina, S. Limpijumnong, B. Segall, and B. K. Meyer, Phys. Rev. B **65**, 075207 (2002).
[17]D. Thomas, J. Phys. Chem. Solids **15**, 86 (1960).
[18]N. Syrbu, I. Tiginyanu, V. Zalamai, V. Ursaki, and E. Rusu, Physica B **353**, 111 (2004).
[19]D. Reynolds, D. Look, and B. Jogai, J. Appl. Phys. **88**, 5760 (2000).
[20]M. Allen, R. Mendelsberg, R. Reeves, and S. Durbin, Appl. Phys. Lett. **94**, 103508 (2009).
[21]G. Blattner, C. Klingshirn, R. Helbig, and R. Meinl, Phys. Status Solidi B **107**, 105 (1981).
[22]M. Hauser, A. Hepting, R. Hauschild, H. Zhou, J. Fallert, H. Kalt, and C. Klingshirn, Appl. Phys. Lett. **92**, 211105 (2008).
[23]N. Ohashi, T. Ohgaki, S. Sugimura, K. Maeda, I. Sakaguchi, H. Ryoken, I. Niikura, M. Sato, and H. Haneda, Mater. Res. Soc. Symp. Proc. **799**, Z5.40 (2004).
[24]D. Bimberg, M. Sondergeld, and E. Grobe, Phys. Rev. B **4**, 3451 (1971).
[25]R. Mendelsberg, J. Kennedy, S. M. Durbin, and R. Reeves, J. Vac. Sci. Technol. B **27**, 1698 (2009).
[26]J. Taylor, *Introduction to Error Analysis*, 2nd ed. (University Science Books, Sausalito, CA, 1997).
[27]M. Schirra, R. Schneider, A. Reiser, G. M. Prinz, M. Feneberg, J. Biskupek, U. Kaiser, C. E. Krill, K. Thonke, and R. Sauer, Phys. Rev. B **77**, 125215 (2008).
[28]U. Fano, Phys. Rev. **124**, 1866 (1961).
[29]K.-J. Jin and S. Xu, Appl. Phys. Lett. **90**, 032107 (2007).
[30]J. Nause and B. Nemeth, Semicond. Sci. Technol. **20**, 45 (2005).
[31]R. Hauschild, H. Priller, M. Decker, J. Brückner, H. Kalt, and C. Klingshirn, Phys. Status Solidi C **3**, 976 (2006).
[32]R. Pässler *et al*., J. Appl. Phys. **86**, 4403 (1999).
[33]C. Boemare, T. Monteiro, M. Soares, J. Guilherme, and E. Alves, Phys. B (Amsterdam) **308-310**, 985 (2001).
[34]L. Viña, S. Logothetidis, and M. Cardona, Phys. Rev. B **30**, 1979 (1984).
[35]A. Manoogian and A. Leclerc, Phys. Status Solidi B **92**, K23 (1979).
[36]G. Wannier, Phys. Rev. **52**, 191 (1937).
[37]P. J. Dean, D. C. Herbert, C. J. Werkhoven, B. J. Fitzpatrick, and R. N. Bhargava, Phys. Rev. B **23**, 4888 (1981).
[38]D. Hamby, D. Lucca, and M. Klopfstein, J. Appl. Phys. **97**, 043504 (2005).
[39]H. Zhao and H. Kalt, Phys. Rev. B **68**, 125309 (2003).
[40]A. Sedhain, J. Li, J. Y. Lin, and H. X. Jiang, Appl. Phys. Lett. **95**, 061106 (2009).
[41]C. Klingshirn, R. Hauschild, J. Fallert, and H. Kalt, Phys. Rev. B **75**, 115203 (2007).
[42]T. Schmidt, K. Lischka, and W. Zulehner, Phys. Rev. B **45**, 8989 (1992).